

# Efficient generation of charges via below-gap photoexcitation of polymer-fullerene blend films investigated by terahertz spectroscopy

P. Parkinson,\* J. Lloyd-Hughes, M. B. Johnston, and L. M. Herz†

*Department of Physics, University of Oxford, Clarendon Laboratory, Parks Road, Oxford, OX1 3PU, United Kingdom*

(Received 15 July 2008; published 24 September 2008)

Using optical-pump terahertz-probe spectroscopy, we have investigated the time-resolved conductivity dynamics of photoexcited polymer-fullerene bulk heterojunction blends for two model polymers: poly[3-hexylthiophene] (P3HT) and poly[2-methoxy-5-(3,7-dimethyloctyloxy)-1,4-phenylenevinylene] (MDMO-PPV) blended with [6,6]-phenyl-C<sub>61</sub> butyric acid methyl ester (PCBM). The observed terahertz-frequency conductivity is characteristic of dispersive charge transport for photoexcitation both at the  $\pi$ - $\pi^*$  absorption peak (560 nm for P3HT) and significantly below it (800 nm). The photoconductivity at 800 nm is unexpectedly high, which we attribute to the presence of a charge-transfer complex. We report the excitation-fluence dependence of the photoconductivity over more than four orders of magnitude, obtained by utilizing a terahertz spectrometer based upon either a laser oscillator or an amplifier source. The time-averaged photoconductivity of the P3HT:PCBM blend is over 20 times larger than that of P3HT, indicating that long-lived hole polarons are responsible for the high photovoltaic efficiency of polymer:fullerene blends. At early times ( $\sim$ ps) the linear dependence of photoconductivity upon fluence indicates that interfacial charge transfer dominates as an exciton decay pathway, generating charges with mobility of at least  $\sim 0.1$  cm<sup>2</sup> V<sup>-1</sup> s<sup>-1</sup>. At later times, a sublinear relationship shows that carrier-carrier recombination effects influence the conductivity on a longer time scale ( $>1$   $\mu$ s) with a bimolecular charge annihilation constant for the blends that is approximately two to three orders of magnitude smaller than that typical for neat polymer films.

DOI: [10.1103/PhysRevB.78.115321](https://doi.org/10.1103/PhysRevB.78.115321)

PACS number(s): 78.30.Jw, 78.66.Qn, 78.55.-m

## I. INTRODUCTION

Organic semiconductors have recently been the subject of intensive research as they offer advantages in processability and ease of band-gap engineering in comparison with conventional inorganic semiconductors.<sup>1-3</sup> In particular, photovoltaic cells incorporating a large-area heterojunction formed between an organic polymers and an electron acceptor have shown external quantum efficiencies of up to 4–6%, and represent a promising technology for future power generation.<sup>4,5</sup> Some of the highest charge-generation efficiencies measured have been produced by blending organic semiconductors such as poly(3-hexylthiophene) (P3HT) or a poly(phenylene vinylene) (PPV) derivative with [6,6]-phenyl-C<sub>61</sub> butyric acid methyl ester (PCBM) (a methanofullerene). These blends have attracted considerable interest because they are very easy to process from solution, making roll-to-roll production of flexible photovoltaics a possibility.<sup>6-9</sup> The primary characteristics required of high-efficiency photovoltaics include: a high photon-to-charge-carrier branching ratio, high carrier mobility, fast electron transfer from charge donor to acceptor, and an absorption spectrum that provides a good balance between dc voltage and harvesting light. It is well known that many factors influence the efficiency of these devices, for example, chain arrangement in the solid,<sup>10</sup> polymer regioregularity,<sup>9</sup> the ratio of polymer to charge acceptor,<sup>11</sup> and postprocess thermal annealing.<sup>8,12</sup> Therefore, for the optimization of photovoltaic device efficiencies, a detailed knowledge of the mechanisms of charge generation and subsequent motion through the material is essential.

A number of studies have attempted to identify the microscopic origin and cause of charge generation and charge-

carrier mobility in organic semiconductors.<sup>13-25</sup> Relatively large carrier mobilities have been proposed; however, there has been disagreement in the literature caused partly by differences between the experimental methods used to investigate carrier dynamics. Measurements carried out on photovoltaic devices, while revealing the real-world behavior of the materials, suffer from difficulties in interpretation arising from the presence of an interface between the electrodes and the polymer.<sup>26</sup> Noncontact measurements, including transient absorption,<sup>13,14</sup> photoluminescence up conversion,<sup>15,27,28</sup> time-resolved microwave conductivity,<sup>16-20</sup> and terahertz time-domain spectroscopy<sup>11,21-25,29,30</sup> have also been used to great effect. A range of values for high-frequency electron and hole mobility from  $10^{-5}$  cm<sup>2</sup> V<sup>-1</sup> s<sup>-1</sup> to over 600 cm<sup>2</sup> V<sup>-1</sup> s<sup>-1</sup> have been proposed for a variety of conjugated polymers; such a large degree of variation suggests that results are very sensitive to both experimental technique and the models used in the analysis.<sup>17,31</sup>

For the study presented here we have used two time-resolved optical-pump terahertz-probe (OPTP) spectrometers to observe the fluence and wavelength dependence of charge generation and carrier mobility in pristine and PCBM-blended organic polymer films. Terahertz time-domain spectroscopy is a unique technique that determines the complex refractive index of a material in the terahertz-frequency range using a single cycle of terahertz radiation as a probe. An electro-optic sampling method is then used to map the time-domain electric field of this probe, providing both spectral amplitude and phase information of the pulse, which may in turn be used to calculate the optical properties of a sample.<sup>32</sup> This technique has advantages over traditional optical-pump optical-probe experiments in that the complex conductivity (at terahertz frequencies) may be calculated

without the need for recourse to the Kramers-Kronig relationship. Using this approach we have been able to measure the complex photoconductivity of two state-of-the-art organic photovoltaic materials, thin films of either P3HT or poly[2-methoxy-5-(3,7-dimethyloctyloxy)-1,4-phenylene vinylene] (MDMO-PPV) blended with PCBM. We examine the dependence of the photoinduced conductivity on time after excitation, frequency of the driving terahertz radiation, and excitation fluence and wavelength. We further discuss the implications of our results for photogeneration efficiencies, and carrier mobilities and lifetimes, and find qualitatively similar results for both polymers investigated.

The OPTP measurements of organic semiconductors reported to date have employed pulsed laser amplifier systems, resulting in high excitation fluences of up to  $6 \text{ mJ cm}^{-2}$ . This approach produces carrier densities in the region of  $10^{21} \text{ cm}^{-3}$ ; however, second-order effects such as bimolecular excitonic or charge annihilation have been shown to occur at carrier densities as low as  $10^{16} \text{ cm}^{-3}$ .<sup>16</sup> In addition, this process inevitably leads to excitation fluences that are many orders of magnitude above those typically encountered under natural conditions such as sunlight. Conclusions drawn from such experiments may therefore have limited applicability to material performance in a typical device structure. We have circumvented this issue by utilizing a low-fluence, high-repetition rate system, which allows us to observe photoinduced conductivity changes for excitation fluences as low as  $24 \text{ nJ cm}^{-2}$  with a good signal-to-noise ratio. In combination with the results derived from an amplifier-based OPTP system, this allows us to examine the photoinduced terahertz conductivity for excitation fluences ranging over more than four orders of magnitude.

A further difficulty encountered with OPTP measurements has been the use of polymer films that are thick in comparison with the absorption depth at optical-pump wavelengths, in order to maximize the absorbed photon fluence and the resulting signal-to-noise ratio.<sup>11,21</sup> However, this practice leads to an exponential distribution of carriers in the direction of terahertz propagation, which complicates the data analysis and extraction of the photoconductivity.<sup>23,33</sup> In the experimental study reported here, we have taken a different approach by exciting with photons of low energy, i.e., significantly below the peak of the  $\pi-\pi^*$  transition of both polymers. Under these conditions a uniformly distributed density of charge carriers is created, whose spectral and temporal OPTP response is remarkably similar to that of charges generated using excitation near the absorption peak. The observation of a low-energy feature in absorption and photoluminescence measurements has recently led to the suggestion that such low-energy photons may create a weakly bound polaron pair formed between the highest occupied molecular orbital (HOMO) of the polymer and the lowest unoccupied molecular orbital (LUMO) of the PCBM.<sup>34</sup> Our measurements reveal a surprisingly high photoconductivity upon excitation of this low-energy feature, suggesting that the polaron pair may offer an efficient direct route to photoexcitation of charges in the polymer blends, in agreement with recent conclusions by Benson-Smith *et al.*<sup>35</sup>

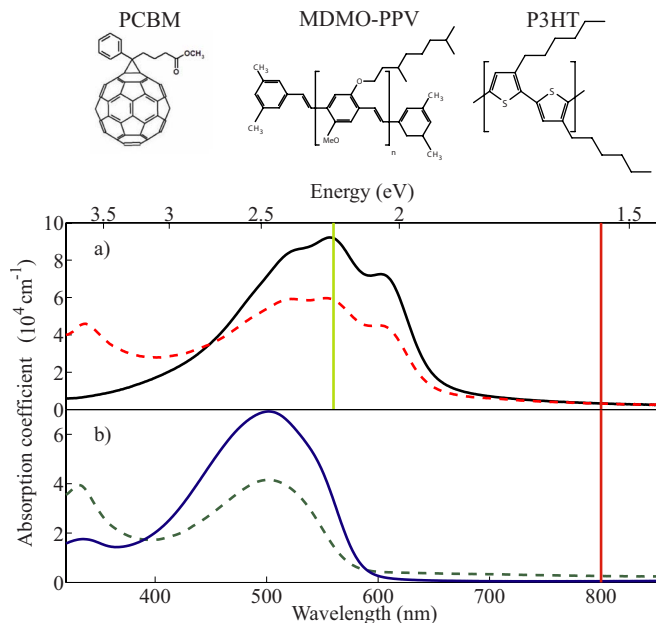


FIG. 1. (Color online) Absorption spectra for thin films of (a) pristine P3HT (black solid line) and the P3HT:PCBM blend (red dashed line), and (b) MDMO-PPV (blue solid line) and the MDMO-PPV:PCBM blend (green dashed line). Vertical lines mark the center wavelengths of the excitation used in the experiments—560 and 800 nm. The chemical structures of the materials used are displayed at the top of the figure.

## II. EXPERIMENT

P3HT ( $M_w=28000u$ ,  $>95\%$  regioregularity), MDMO-PPV ( $M_w=718000u$ ), and PCBM were purchased from *American Dye Source* and used without further purification. The chemical structures of all components can be found at the top of Fig. 1. Each material was separately dissolved in dichlorobenzene at a concentration of  $15 \text{ g l}^{-1}$  and polymer-fullerene blends were derived by mixing the relevant solutions at a 1:1 ratio by volume. To produce films, the solutions were spin cast or drop cast onto *z*-cut quartz substrates for optical-density measurements or terahertz measurements, respectively. Thick ( $d \sim 10 \text{ }\mu\text{m}$ ) drop-cast samples were required for the terahertz measurements to ensure sufficiently high photoinduced conductivity for the case when the photon-to-charge branching ratio was small (e.g., for the pristine unblended samples). All samples were dried and annealed at  $100 \text{ }^\circ\text{C}$  for 3 h. Materials were handled and samples were prepared in an inert ( $\text{N}_2$ ) atmosphere. Thin-film transmission measurements were performed using a spectrophotometer (Perkin-Elmer Lambda 9), and the film thickness was measured using a step profilometer (Veeco DekTak 7).

Optical-pump terahertz-probe measurements were taken using two different terahertz spectrometers. The high-fluence spectrometer used a regenerative amplifier (800 nm center wavelength, 1 kHz repetition rate, 50 fs pulse duration, and 1 mJ pulse energy). The terahertz probe was generated through optical rectification in a 2-mm-thick ZnTe crystal, and detected using electro-optic sampling in a 1-mm-thick ZnTe crystal. Photoexcitation of the sample was carried out either

using up to 500  $\mu\text{J}/\text{pulse}$  of the 800 nm fundamental, or the output from a TOPAS optical parametric amplifier, providing around 30  $\mu\text{J}/\text{pulse}$  at 560 nm. To measure the low-fluence photoconductivity, a Ti:sapphire laser oscillator (800 nm center wavelength, 80 MHz repetition rate, 100 fs pulse duration, and 12 nJ pulse energy) was used both to photoexcite the sample, and to generate and measure the terahertz probe. The terahertz probe was generated in a biased photoconductive switch, and measured using electro-optic sampling in a 2-mm-thick ZnTe crystal—full details of this setup are provided in Ref. 36. All measurements were made under vacuum ( $<10^{-3}$  mbar) to minimize photo-oxidization; no sample degradation was seen during these experiments.

In an optical-pump terahertz-probe experiment, the photo-induced change in the transmitted terahertz electric-field amplitude,  $\Delta T/T$ , is measured also as a function of pump-probe delay. The following relatively simple calculation derived from thin-film optics allows reconstruction of the photoinduced change in sample conductivity  $\Delta\sigma$  from this change in transmission  $\Delta T/T$ , only requiring knowledge of the excited sample thickness  $d$  and the substrate refractive index  $n$ :<sup>37</sup>

$$\Delta\sigma = \frac{1+n}{Z_0 d} \left( \frac{1}{1+\Delta T/T} - 1 \right), \quad (1)$$

where  $Z_0$  is the impedance of free space. For excitation at 800 nm, a uniform distribution along the sample depth is created and  $d$  represents the film thickness. For excitation at 560 nm, a uniformly excited block, as thick as the penetration depth  $d$ , was assumed to exist upon an unexcited P3HT substrate.<sup>38,39</sup> For ease of examination, the experimental results shown throughout this report were converted from the measured  $\Delta T/T$  to photoinduced conductivity units. Both of the principal modes of operation of the optical-pump terahertz-probe experiment were employed for the measurements; in the following these are referred to as *fixed-gate* and *fixed-pump* modes. For the fixed-gate mode, the photoinduced change in peak terahertz transmission, which is related to the frequency-averaged photoinduced conductivity of the sample, is measured as a function of pump-probe delay. The resulting curves are measures of the transient conductivity as a function of time after excitation, and may yield information on free-carrier lifetimes and the evolution of the charge mobility. Additional information can be extracted through operating the experiment in fixed-pump mode—here, the photoinduced change in terahertz time-domain electric field is measured at a fixed-pump delay. From this measurement, the real and imaginary parts of the photoconductivity spectrum across the terahertz range can be determined for a set time after excitation of the sample.

Figure 1 shows the thin-film absorbance spectra for pristine and PCBM-blended P3HT and MDMO-PPV. For both polymers, the addition of PCBM introduces a characteristic absorption at 340 nm. In the present paper, we will distinguish between photoexcitation with energy above and below the polymer absorption onset as *above gap* and *below gap*, respectively. Knowledge of the absorption depth coupled with the incident optical-pump fluence and sample thickness permits calculation of the initial photoexcitation density.

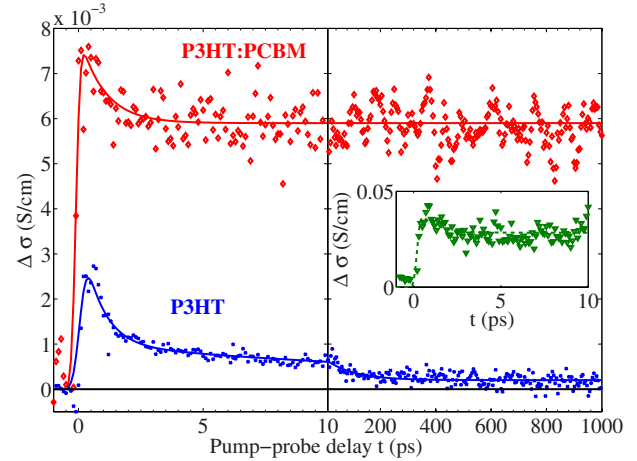


FIG. 2. (Color online) Photoinduced change in conductivity for thin films of pristine P3HT (blue circles) and P3HT:PCBM (red diamonds) as a function of time after excitation with an 800 nm optical pulse at a fluence of 425  $\mu\text{J cm}^{-2}$ . The inset shows the photoinduced change in conductivity of the blend after excitation with a 560 nm optical pulse at a fluence of 210  $\mu\text{J cm}^{-2}$ . Lines shown are a guide to the eye.

However, at the low-energy tail of the displayed spectra, the measured nonzero absorbance is most likely dominated by the result of scattering from the film rather than electronic transitions in the material. Fourier-transform photocurrent spectroscopy is a technique that allows more accurate absorption measurements with larger dynamic range. Recent results using this technique have demonstrated the existence of a subgap absorption feature near 800 nm for P3HT:PCBM blends.<sup>34</sup> In order to obtain a correct measure of the photoinduced excitation density for the study presented here, the thin-film absorbance measurements shown in Fig. 1 were used for above-gap excitation while for below-gap excitation the absorbance was derived from the Fourier-transform photocurrent measurements of Ref. 34. The reported absorption coefficient at 800 nm was 10  $\text{cm}^{-1}$  for P3HT, 200  $\text{cm}^{-1}$  for P3HT:PCBM, 2  $\text{cm}^{-1}$  for MDMO-PPV, and 180  $\text{cm}^{-1}$  for MDMO:PCBM.<sup>34</sup>

### III. RESULTS

Figure 2 shows the time-resolved conductivity of both P3HT and P3HT:PCBM blends after photoexcitation at 800 nm, extracted using the fixed-gate method. These curves were obtained by using the high-fluence, low repetition rate system. Both samples show a sharp rise in photoinduced conductivity immediately after excitation, starting from a value near zero. These curves demonstrate that for both samples, the lifetime of photoexcitations in the material is significantly shorter than the interpulse separation (1 ms), and that at these photon fluences photoconductivity arises within the temporal resolution of the system ( $\sim 300$  fs).

The initial amplitude of the photoinduced conductivity is surprisingly similar for both materials given that one might expect the presence of the electron acceptor PCBM to enhance the generation of charges in the polymer considerably.

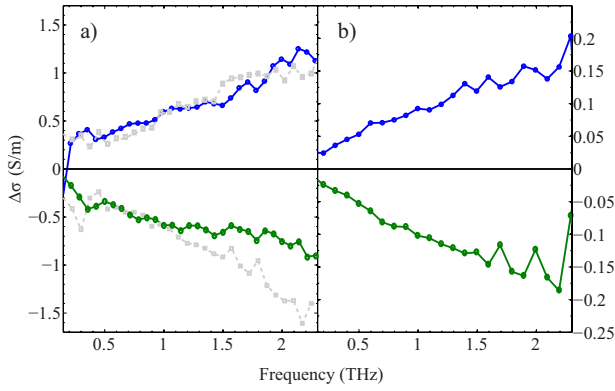


FIG. 3. (Color online) Photoinduced conductivity spectra across in the terahertz region for the P3HT:PCBM film (a) taken on the high-fluence amplifier system at 1.2 ns after excitation with 800 nm photons of fluence  $425 \mu\text{J cm}^{-2}$  (blue and green lines and circles) and after excitation with 560 nm photons of fluence  $210 \mu\text{J cm}^{-2}$  (gray dashed lines and squares, divided by ten to allow comparison); (b) taken on the low-fluence oscillator system after excitation with 800 nm photons of fluence  $0.64 \mu\text{J cm}^{-2}$  for a nominal delay time of 10 ps.

Comparable observations have been made by other groups using high excitation fluences but exciting nearer the peak of the polymer absorption spectrum. Ai *et al.*<sup>11</sup> found initial photoinduced terahertz conductivities that were within an order of magnitude for a range of P3HT:PCBM films with PCBM content varying between 0 and 80% by weight, while Hendry<sup>33</sup> observed the initial photoconductivity of a PPV derivative blended with 50% PCBM to be approximately six times larger than that for the pristine film. More recently Cunningham and Hayden<sup>25</sup> observed very little change in peak photoconductivity upon the addition of PCBM. However, it is the subsequent evolution of the photoconductivity that reveals the difference between the pristine polymer and the bulk heterojunction blend. In P3HT the conductivity decreases rapidly over the first few picoseconds and subsequently decays according to the power law  $\Delta\sigma \propto t^{-\beta}$  with  $\beta = 0.31 \pm 0.03$ . This kind of power-law decay is a signature of the dispersive transport of charges in disordered media.<sup>40</sup> In contrast, the conductivity dynamic in the P3HT:PCBM blend is significantly slower, with a lifetime substantially longer than the  $\sim 1$  ns range of our experiment.

The photoinduced conductivity for the P3HT:PCBM film under photoexcitation at the  $\pi-\pi^*$  absorption peak (560 nm) is shown in the inset to Fig. 2. The dynamics are qualitatively identical to those seen when 800 nm excitation is used, suggesting that the same species is photoexcited under both excitation conditions. To garner further information about the photoexcited species created in both case, a fixed-pump measurement was taken at 1.2 ns delay after excitation, at which time the system has entered a quasiequilibrium state. Figure 3(a) shows the terahertz-frequency spectra of the photoinduced conductivity for the P3HT:PCBM film after excitation at 800 and 560 nm. The spectral signature of the conductivity response is almost identical for both excitation wavelengths, again indicating that the same type of species is generated for above-gap and below-gap excitations, at high fluences.

For inorganic semiconductors<sup>41</sup> and heavily doped polymers,<sup>42,43</sup> the Drude model of free carriers has been

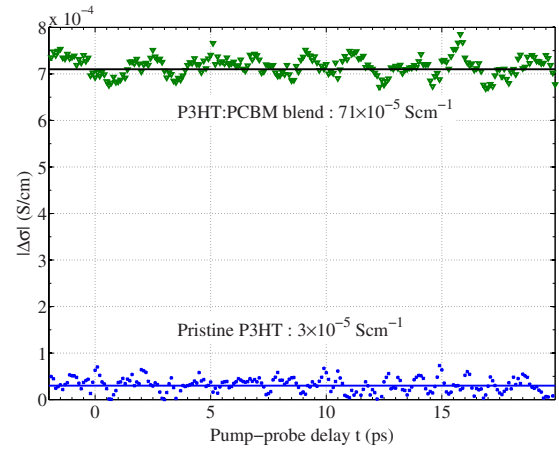


FIG. 4. (Color online) Photoinduced change in conductivity for pristine P3HT and P3HT:PCBM blend films as a function of time after excitation at 800 nm using the low-fluence ( $0.64 \mu\text{J cm}^{-2}$ ), high-repetition rate system. No rise in photoconductivity can be observed at zero delay (corresponding to the arrival of the excitation pulse), indicating that the photoconductivity lifetime is significantly longer than the laser interpulse period ( $\Delta t = 12.5$  ns).

found to model the terahertz conductivity accurately. The observed monotonic increase in the real and imaginary parts of the conductivity in Fig. 3(a) is in clear disagreement with the Drude model, which predicts a maximum in the real part of the conductivity at  $\omega=0$  and a positive imaginary component peaked at the inverse scattering time of the carriers. Similar conductivity spectra have been recently reported for polymer:fullerene blends using high excitation fluences near the peak of the polymer absorption spectrum.<sup>11,21,23,30</sup> The microscopic origin for the terahertz photoconductivity spectra of semiconducting polymers is currently a well-debated issue in the literature. It has been suggested that such terahertz-frequency response may arise from a charge conductivity limited by torsional disorder along the polymer backbone,<sup>44</sup> or from the backscattering of charges from the ends of conjugated segments, leading to a maximum in the conductivity at nonzero frequency<sup>11</sup> as described in the Drude-Smith model.<sup>45</sup> Additionally, the terahertz-frequency conductivity of polarons in polymer blends has been modeled as a Debye relaxation process.<sup>30</sup> In order to distinguish between these competing models, THz-TDS (time-domain spectroscopy) experiments are required at frequencies higher than 2.5 THz (the maximum frequency accessible in our study, and also in those presented in Refs. 11, 25, and 29).

Figure 4 shows the photoinduced conductivity for P3HT and P3HT:PCBM films as a function of time after excitation at 800 nm, measured with the laser oscillator system at an excitation fluence roughly three orders of magnitude below that used to acquire the curves shown in Fig. 2. In order to obtain a sufficiently high signal-to-noise ratio at such low fluences using current techniques, it is inevitable that higher pulse repetition rates be used. As a result, no increase in photoconductivity is now seen at  $t=0$  ps, suggesting that the predominant species present on time averaging has a lifetime that exceeds the interpulse separation of the laser oscillator (12.5 ns) by a significant amount. For example, if we as-

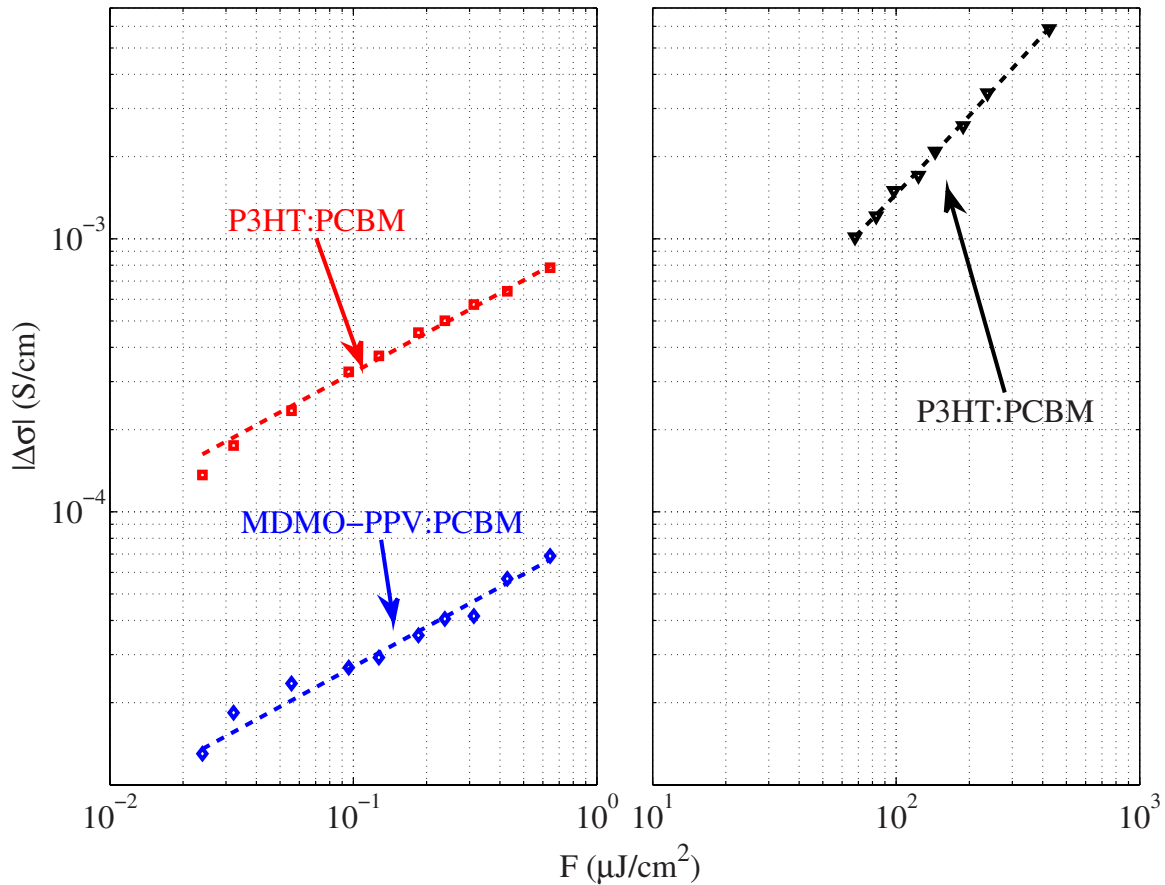


FIG. 5. (Color online) Fluence dependence of the photoinduced change in conductivity at 800 nm for MDMO-PPV:PCBM (blue diamonds) and P3HT:PCBM (red squares) measured with the low-fluence system, and for P3HT:PCBM measured with the high-fluence system (black triangles). For the low-fluence regime, the data points are the average of photoconductivity transients measured in the nominal delay range of 2–20 ps (as shown, e.g., in Fig. 4), while for the high-fluence regime the average was taken over the long-term delay scans between 0.08–1.2 ns (as displayed in the right panel of Fig. 2). Both methods yield the spectrally averaged value of the terahertz photoconductivity for the times at which the spectrum carries a charge-carrier signature. The low-fluence data represent a time-averaged photoconductivity value while the high-fluence data corresponds to the charge yield before recombination. The lines shown are power-law fits yielding approximately square root and linear dependencies for low-fluence and high-fluence experiments, respectively, as described in the text.

summed for simplicity that only one species was present, which decayed exponentially, then its lifetime would need to exceed  $\sim 100$  ns in order for us not to resolve a rise near zero delay within our signal fluctuations. The long-lived nature of the species strongly suggests that the low-fluence measurements predominantly probe free charges in the material. This conclusion is supported by the fact that a significant increase ( $\times 24$ ) in the conductivity can be observed when PCBM is added to P3HT. P3HT:PCBM photovoltaic devices are known to exhibit good external quantum efficiency,<sup>5</sup> and it is therefore to be expected that the primary time-averaged photoexcited species in these materials are free charge carriers. In order to determine the terahertz signature of free charges in the polymer, the photoinduced conductivity spectrum was taken for the P3HT:PCBM film, as shown in Fig. 3(b). Comparison with the data taken on the high-fluence system unambiguously confirms that, for all three types of measurement, i.e., at 1 ns after excitation below gap or above gap with high fluence, and on time-average after excitation below gap with low fluence, the predominant

species causing a change in terahertz transmission for P3HT:PCBM films are free charges. In Sec. IV we discuss further the possible charge-generation mechanisms for polymers and polymer:fullerene blends photoexcited above and below the  $\pi-\pi^*$  absorption edge.

Using both high-fluence and low-fluence OPTP systems, we were able to assess the fluence dependence of the photoinduced conductivity, which may provide information about charge-carrier generation and carrier-carrier scattering mechanisms, and about the trap density in the material.<sup>16,46</sup> Such measurements are particularly useful to attempt to relate the photovoltaic efficiency measured in a high-fluence laboratory setting to a real-world (air mass 1.5) environment. Figure 5 shows the spectrally and temporally averaged photoconductivity as a function of excitation fluence  $f$  for P3HT:PCBM and MDMO-PPV:PCBM blends photoexcited at 800 nm. From the double-logarithmic representation, it can be seen that the fluence dependence of the conductivity follows a power law of the form  $|\Delta\sigma|=Af^B$ . Best fits to the data are shown as lines in the graph, and yield an approxi-

mate dependence of the photoconductivity upon the square root of the fluence for P3HT:PCBM and MDMO-PPV:PCBM within the low-fluence regime ( $B=0.48 \pm 0.01$  and  $B=0.49 \pm 0.01$ , respectively), and a linear dependence ( $B=0.98 \pm 0.02$ ) for P3HT:PCBM at high fluences. However, while the two polymers investigated show a similar fluence dependence of the photoconductivity, its overall value is larger for P3HT than for MDMO-PPV by approximately an order of magnitude. The implications of the fluence dependence of the terahertz photoconductivity for the blend films on the mechanisms of charge-carrier generation and recombination are examined in detail in the Sec. IV below.

#### IV. DISCUSSION

In this section we aim to place the present and previous results from OPTP spectroscopy of polymeric semiconductors in the context of reported charge generation and transport mechanisms in these materials. The absorption of a photon by a  $\pi$ -conjugated polymer begins a chain of events that may result in charge generation. In neat polymer films, Coulombically bound-electron-hole pairs (excitons) are the primary species created at low photoexcitation densities with a photon-to-charge ratio  $\phi$  of typically less than 1%.<sup>18</sup> In P3HT:PCBM blend films,  $\phi$  may be as large as 30%, facilitating the use of this blend in high-efficiency organic photovoltaic devices.<sup>47</sup> Once created, excitons may migrate either along a polymer chain by hopping to neighboring conjugated segments, between chains, or into a charge-separated state. Alternatively, excitons may decay via a radiative or nonradiative process. A charge-separated state is one in which the (still-bound) electron and hole become separated between two conjugated segments, or over an interface.<sup>27,28</sup> In these states, it is possible that an energy mismatch between segments or components may help to overcome the exciton binding energy.<sup>48–50</sup> In the case of a P3HT:PCBM blend, charge separation has been proposed to occur predominantly at the bulk interface between the polymer and the fullerene, generating an electron on the PCBM and the hole on the polymer.<sup>6</sup> Using the above-gap and below-gap excitation dynamics, and spectral conductivity “fingerprint” presented above, we now discuss in more detail the charge generation and recombination mechanisms in these polymer-fullerene blends. Subsequently, we estimate lower bounds to the mobility  $\mu$  and bimolecular annihilation constant  $\gamma$  of charge carriers by calculating the products  $\phi\mu$  and  $\phi\gamma$  from the measured fluence dependencies of the photoconductivity.

##### A. Carrier generation and recombination

The origin of the induced conductivity for photoexcitation at energies significantly below the peak of the  $\pi-\pi^*$  absorption needs further consideration. Below, we divide the discussion of the possible carrier generation mechanisms into those applicable at low and high photon fluence, and consider the changes that occur on blending neat P3HT with PCBM.

Charge generation routes that are intrinsic to neat conjugated polymer solids have been discussed in much detail in

the literature.<sup>51–56</sup> For the below-gap excitation of P3HT films, as carried out in the present study, it is possible that electronic states are excited in the low-energy tail of the distribution, corresponding to very long conjugated polymer segments. The small yet finite absorbance of the samples at 800 nm suggests that this is feasible, in particular, given the large thickness of the films. However, such states would have the minimum energy required for the generation of an exciton in the material while a number of theoretical models indicate that an excess energy may be required for an exciton to dissociate into charges. Such excess energy may, for example, lead to a larger initial separation between electron and hole,<sup>57</sup> which according to the Onsager model<sup>58</sup> will lead to a higher charge separation probability. Excess vibrational energy associated with the polymer backbone has also been postulated to enhance the on-chain dissociation probability.<sup>55</sup> In addition, the energetic mismatch between adjacent sites in the inhomogeneously broadened density of states present in the films may be utilized to overcome the barrier to charge separation of the exciton.<sup>51–53</sup>

However, a number of studies on polythiophene films have demonstrated that these materials do not comply with such models and instead show charge-generation efficiencies that are essentially independent of the energy of the exciting photons across the lowest electronic transition band.<sup>13,59,60</sup> This effect has been attributed to either the presence of an ordered lamellar structure in regioregular P3HT (Ref. 59) or the availability of special “dissociation sites” comprising of chain kinks, twists, or aggregates.<sup>13,61</sup> Here, the former study proposed an intrinsic charge separation efficiency of 2% while the latter two concluded it to be as high as 13–20% within the lowest absorption band. According to these studies, direct intrinsic photogeneration of charges should be expected to occur to a significant extent for the P3HT films under investigation here.

Intrinsic charge generation cannot, however, be the only mechanism in operation as the addition of PCBM to P3HT is found to increase the initial photoconductivity even though the density of P3HT spectroscopic units is reduced (Fig. 2). Therefore, extrinsic mechanisms for charge generation in P3HT introduced through the addition of the electron acceptor PCBM also need to be considered. For the case of polymer-fullerene blends, a specific charge-transfer state has recently been identified as an extrinsic, below-gap route to charge photogeneration. This directly accessible state with less than  $\sim 1.5$  eV excitation energy was found to be present in P3HT:PCBM and MDMO-PPV:PCBM blends, and absent in pristine P3HT, MDMO-PPV, or PCBM films.<sup>34</sup> Similar effects have also been noted in polyfluorene-fullerene blends.<sup>35,49</sup> It was subsequently suggested that the relevant features in the absorption correspond to a weakly bound polaron pair, as they occur concomitantly with efficient charge photogeneration.<sup>34,35</sup> The final product of exciting these sub-gap features would thus be a charge-separated state such as a free polaron, with an electron transferring to the PCBM and the hole remaining on the polymer chain.<sup>6,48</sup> Using ultrafast transient absorption, Hwang *et al.*<sup>62</sup> have recently shown that, for P3HT:PCBM blends, a charge-transfer state exists, operating as an intermediate state between the photoexcitation of an exciton and free polaron conductivity. Such a state

was not observed in pristine P3HT films. The high photoinduced terahertz conductivity we measure for below-gap excitation of these blends across all excitation fluences strongly suggests that such direct excitation of a subgap charge-transfer state is a principal mechanism contributing to charge generation here.

Ultrafast (<100 fs) charge generation in conjugated polymeric films at high excitation fluences has been reported on a number of occasions<sup>56,63–68</sup> with the mechanisms remaining the subject of much controversy. For example, it has been suggested that a two-step, two-photon absorption to specific higher-lying even-parity states in polyphenylene vinylene may lead to subsequent efficient relaxation of the exciton into a charge-separated state.<sup>63</sup> At high excitation densities, such states may be accessed by sequential two-photon absorption within the duration of the excitation pulse, leading to a superlinear dependence of the charge-generation efficiency on excitation fluence. For example, Silva and co-workers<sup>56,68</sup> have used photoinduced absorption measurements to show that the only route to photogeneration of polarons in thin films of a polyindenofluorene derivative is via such two-step excitation processes. Alternatively, Müller *et al.*<sup>66</sup> have postulated that these two-step photon absorption processes in neat polymer films generate a fraction of bound polaron pairs as a first step, whose subsequent reexcitation by a second photon pulse leads to their dissociation into free charges. Interestingly, a subsequent study by the same authors showed that, for efficient polymer:PCBM photovoltaic blend films, such initial bound polaron pairs are absent and therefore the arrival of a second pulse is unable to generate further free charges.<sup>67</sup> Both of the postulated mechanisms for direct, two-step charge photogeneration will thus lead to a superlinear increase in the charge-generation efficiency for neat polymer films with photon fluence. However, for efficient donor-acceptor blends, a linear fluence dependence of the photon-to-charge conversion efficiency may occur if extrinsic mechanisms at the heterojunction become the dominant pathway to charge generation.

In addition to the fluence dependence of the initial generation of charges, the subsequent recombination of charges has also to be considered. Here, bimolecular charge-carrier recombination dynamics may lead to a sublinear dependence of the time-dependent charge population with excitation fluence. Previous studies of microwave conductivity on P3HT:PCBM films noted an onset of bimolecular charge-carrier recombination at an incident photon fluence of around  $5 \times 10^{12} \text{ cm}^{-2}$  but did not report any evidence of two-photon effects for fluences up to  $10^{15} \text{ cm}^{-2}$ .<sup>16</sup> In a similar study, Dicker *et al.*<sup>59</sup> used time-resolved microwave conductivity measurements on thin films of P3HT to demonstrate that the photoconductivity increases sublinearly over the range of  $10^{13}$ – $4 \times 10^{15} \text{ cm}^{-2}$ , attributing this to secondary processes (e.g., bimolecular charge recombination). An OPTP measurement taken on P3HT:PCBM blend films using a 500 nm optical pump in the range of  $2.5 \times 10^{14}$ – $2 \times 10^{15} \text{ cm}^{-2}$  also shows an initial sublinear fluence dependence of photoconductivity with excitation power (over the time range of  $1 < t < 75 \text{ ps}$ ), in agreement with bimolecular charge generation occurring already within the duration of the excitation pulse.<sup>11</sup>

The incident fluence used in the experiments reported here ranged from  $9 \times 10^{10}$ – $1.7 \times 10^{15} \text{ cm}^{-2}$  per pulse at 800 nm; therefore, all of the excitation processes discussed above are likely to contribute to some extent. In order to make a qualitative statement on their relative importance, we have measured the fluence dependence of the terahertz photoconductivity signal over more than four orders of magnitude, which we now discuss in more detail.

### B. Dependence of charge-carrier conductivity on excitation fluence

An ultimate goal of the spectroscopic analysis of organic photovoltaic materials is to understand both the charge-generation method and to find an appropriate model for carrier mobility. However, without independent knowledge of the photon-to-charge branching ratio  $\phi$  and in absence of a universally accepted model for high-frequency charge mobility  $\mu$ , we can only compare the product of these two quantities. In the following we will examine the differences in fluence dependence of the photoconductivity observed for the two fluence regimes, and use this information to assess charge mobility and recombination in the material.

Figure 5 illustrates a marked contrast between the low-fluence and high-fluence photoconductivity data measured for P3HT:PCBM films. As stated in Sec. III, the data can be well modeled for both fluence regimes using a power-law function, with the low-fluence regimes displaying a square root and the high-fluence regime displaying a linear dependence of photoconductivity upon incident fluence. However, for a meaningful comparison of the data sets taken within the two regimes, one has to consider that the high-fluence photoconductivity is measured over the first nanosecond after excitation whereas the low-fluence data is essentially an average over the whole charge lifetime. For the high-fluence regime, the photoconductivity displayed in Fig. 5 is an average over 0.08–1 ns after excitation, for which a constant value is observed in the conductivity dynamics (see Fig. 2). These data thus represent the conductivity state of the material *after* the initial charge-generation processes have occurred within the first few picoseconds but *before* any significant charge-carrier decay has occurred. The low-fluence data, on the other hand, is strongly influenced by “wrap-around” effects: the lack of any stepwise increase in the photoconductivity at  $t=0$  (see Fig. 4) demonstrates that a significant photoexcited charge population remains after 12.5 ns, the interpulse period of the laser. A meaningful comparison with the high-fluence data is only possible if the evolution of the conductivity signal beyond 1 ns after excitation is known, as the low-fluence data must then be corrected for the buildup of carriers from previous excitation pulses.

In general, the photoconductivity of the blend is given by  $\Delta\sigma=Nq\mu$ , where  $N$  is the carrier density,  $q$  is the electronic charge, and  $\mu$  is the effective carrier mobility for the conductive polaron species. For the *high-fluence* data, the linearity of the photoconductivity power dependence suggests that extrinsic charge generation at the P3HT:PCBM heterojunction is the primary mechanism for initial photon-to-charge conversion even at fluences as high as  $500 \mu\text{J cm}^{-2}$ . An ini-

tial (picosecond) value of  $\phi\mu$  may then be extracted from the high-fluence measurements of the initial photoconductivity  $\Delta\sigma_0$  using

$$\phi\mu = \frac{\Delta\sigma_0}{qn_0^{\text{photon}}}, \quad (2)$$

where  $n_0^{\text{photon}} = (1 - e^{-\alpha d})I_0/d$  is the initially generated average photon density derived from the absorption coefficient  $\alpha$ , the sample thickness  $d$ , and the number of photons  $I_0$  incident per unit area. Using this approach, we determine a value of  $\phi\mu = 0.11 \text{ cm}^2 \text{ V}^{-1} \text{ s}^{-1}$  for excitation at 800 nm by performing a linear fit to the fluence dependence of the conductivity shown in the right side of Fig. 5.

To interpret the *low-fluence* conductivity data, it has to be taken into account that the carrier density is built up by successive pulses creating the wrap-around effect mentioned in the previous paragraph. The sublinear fluence dependence observed could be caused by nonlinear effects in the charge generation and/or recombination processes. However, the linear fluence dependence of the photoconductivity in the high-fluence regime suggests that the latter is the case. We therefore follow the treatment outlined by Dicker *et al.* in Ref. 59 and write the rate of change of carrier density, taking into account a bimolecular decay route, as

$$\frac{dN}{dt} = \frac{\phi n_0^{\text{photon}}}{\Delta t} - \gamma N^2, \quad (3)$$

where  $\gamma$  is the bimolecular charge annihilation constant. Since the interpulse separation  $\Delta t = 12.5 \text{ ns}$  is significantly shorter than the charge lifetime for our present case, the steady-state charge density  $N_\infty$  leading to the observed photoconductivity is given by  $N_\infty = \sqrt{\phi n_0^{\text{photon}} / (\Delta t \gamma)}$ . Since we indeed observe a dependence of photoconductivity on the square root of excitation fluence, such bimolecular charge annihilation effects appear to be the predominant mechanism for the photoconductivity decay over the lifetime of the charge species both in P3HT:PCBM and MDMO-PPV:PCBM blend films. The product  $\phi\gamma$  of the photon-to-charge branching ratio and the bimolecular charge annihilation constant may then be written as

$$\phi\gamma = \frac{n_0^{\text{photon}}}{\Delta t} \left( \frac{q\phi\mu}{\Delta\sigma} \right)^2. \quad (4)$$

By performing a square-root fit to the low-fluence photoconductivity data for P3HT:PCBM blends (Fig. 5, left), we hence extract a value of  $\phi\gamma = 1.94 \times 10^{-11} \text{ cm}^3 \text{ s}^{-1}$  using the high-fluence value of  $\phi\mu = 0.11 \text{ cm}^2 \text{ V}^{-1} \text{ s}^{-1}$ .

Since the photon-to-charge branching ratio must be smaller than one, the above considerations provide lower limits to the charge mobility and bimolecular charge annihilation constant of  $0.11 \text{ cm}^2 \text{ V}^{-1} \text{ s}^{-1}$  and  $1.94 \times 10^{-11} \text{ cm}^3 \text{ s}^{-1}$ , respectively, for photoexcitation of P3HT:PCBM blends at 800 nm. However, as previous studies have suggested a high initial photon-to-charge conversion ratio for such blend systems,<sup>11,69</sup> these values are likely to be of the same order of magnitude as the actual charge mobility and bimolecular annihilation constant. As previously reported,<sup>11</sup> the early time conductivity dynamic ( $< 1 \text{ ns}$ ) of-

ten differs significantly from the later time dynamic as the competition between the possible decay routes varies; i.e., between charge recombination at an interface and polaron-polaron annihilation. In our case, the high-fluence data provides an early time measurement in which exciton dissociation at a P3HT:PCBM interface dominates while the low-fluence data represents a time-averaged measurement over the lifetime of the photoexcited species for which polaron-polaron annihilation is the primary decay route.<sup>59</sup>

To compare these values with those recorded under above-gap photoexcitation, the product  $\phi\mu$  was extracted from the photoconductivity data shown in the inset of Fig. 2, as measured for excitation at 560 nm with a fluence of  $210 \mu\text{J cm}^{-2}$ . We obtain  $\phi\mu_{560 \text{ nm}} = 0.072 \text{ cm}^2 \text{ V}^{-1} \text{ s}^{-1}$  at 5 ps after excitation, somewhat smaller than the value at 800 nm of  $\phi\mu_{800 \text{ nm}} = 0.11 \text{ cm}^2 \text{ V}^{-1} \text{ s}^{-1}$ . If similar carrier mobilities for the charge-separated state produced after the photoexcitation of excitons at 560 nm and the photoproduct at 800 nm were assumed, this would imply that the charge-generation efficiency is surprisingly high when the charge-transfer state is excited resonantly. For actual photovoltaic devices incorporating thin ( $d \approx 100 \text{ nm}$ ) films, this charge-transfer state may however still not provide a major route toward photocurrent generation as the associated subgap absorption appears to be relatively weak.<sup>34</sup>

The lower limit of  $1.94 \times 10^{-11} \text{ cm}^3 \text{ s}^{-1}$ , we find for the charge annihilation rate is significantly lower than values for  $\gamma$  found previously for neat polymer films: For both neat P3HT (Ref. 59) and poly(phenylene vinylene),<sup>26</sup> a value of  $\gamma$  has been determined to be  $\sim 1 \times 10^{-8} \text{ cm}^3 \text{ s}^{-1}$ . For P3HT it was suggested that the value correlates with the charge-carrier density for which there appear to be a significantly high number of lamella with two carriers present, leading to efficient charge annihilation within a lamella.<sup>59</sup> The value we determine for the blend is approximately two to three orders of magnitude smaller than those seen for neat polymer films, which should be expected since it is the interface surface forming the heterojunction between P3HT and PCBM that will influence the probability of an encounter between oppositely charged polarons in the blend, thus lowering the probability of bimolecular charge recombination. This contrast between the charge recombination in neat and blend films is self-evident from the conductivity dynamics for the two materials displayed in Fig. 2. For the Langevin model, recombination is assumed to arise from a strictly random process that is kinetically bimolecular.<sup>50</sup> In this case, the recombination coefficient can be related directly to the carrier mobility and dielectric constant of a material through

$$\frac{\gamma}{\mu} = \frac{e}{\epsilon_0 \epsilon_r}. \quad (5)$$

For a terahertz-frequency dielectric constant of  $\epsilon_r = 10.4$ ,<sup>38,39</sup> a predicted value of  $\gamma/\mu = 1.74 \times 10^{-7} \text{ cm V}$  is thus obtained for this model. By dividing our experimentally determined values for  $\phi\gamma$  and  $\phi\mu$ , we obtain a value of  $\gamma/\mu = 1.76 \times 10^{-10} \text{ cm V}$ , which is significantly smaller than that predicted by Langevin recombination. As our terahertz-frequency mobility values are less than or equal to those previously reported in the literature, the deviation is likely to

arise from a bimolecular recombination coefficient that cannot be adequately described by Langevin processes. Similar observations have previously been made for P3HT:PCBM bulk heterojunctions by Juška and co-workers<sup>70,71</sup> using a device-based technique. This suggests that, independently of the frequency of the probing electric fields, the intrinsic recombination process in P3HT:PCBM blends does not follow the simple Langevin theory most probably because it is strongly influenced by the shape of the interface between the two materials.

The values of  $\phi\mu$  we report here are approximately an order of magnitude larger than those observed using the time-resolved microwave conductivity technique with a similar excitation fluence.<sup>16,72</sup> This observation is in accordance with the frequency spectrum of the conductivity displayed in Fig. 3 from which a significant conductivity drop toward microwave frequency should be expected. The mobility and quantum efficiency values reported by both Ai *et al.*,<sup>11</sup> and Cunningham and Hayden<sup>25</sup> using OPTP are significantly larger than those presented here. This is likely to be a result of the use of Drude-Smith modeling in these studies as the presence of a strong backscattering parameter requires that a larger carrier mobility must be used to explain a given conductivity.

Finally, we also determined the product  $\phi\mu$  for neat P3HT films photoexcited at 800 nm at very high fluences ( $425 \mu\text{J cm}^{-2}$ ) to be  $\phi\mu=0.073 \text{ cm}^2 \text{ V}^{-1} \text{ s}^{-1}$ . This value is only slightly below that determined for the P3HT:PCBM blend films, and therefore surprisingly high given that the addition of PCBM is expected to increase significantly the quantum efficiency of charge generation. If the photon-to-charge branching ratio were indeed significantly lower for the neat film than for the blend, a strong reduction in charge mobility would be required upon blending in order to achieve the observed values of  $\phi\mu$ . The addition of PCBM should decrease the mobility of carriers in P3HT to some extent<sup>73</sup> as the polymer:fullerene heterojunction is most effective where the microcrystalline phases in the blend are around 5–10 nm in size.<sup>67,74</sup> However, recent investigations of P3HT:PCBM blend films indicate that self-organization of P3HT into ordered domains is still effective even in the presence of 50 wt % PCBM.<sup>75</sup> Any decreases in mobility with blending are thus likely to be small, suggesting that  $\phi$  for the neat P3HT film cannot be much lower than that for the blend, at the high photon fluences used for excitation here. It is therefore likely that in the high-fluence regime, additional nonlinear mechanisms of charge generation, as discussed in

detail the previous section, are in operation for neat P3HT. However, the linear increase in the initial photoconductivity with excitation fluence we observe for P3HT:PCBM films suggests that, for these, a direct photogeneration of charges at the heterojunction is the predominant mechanism, in agreement with the interpretation by Müller *et al.*<sup>67</sup> of transient absorption and photocurrent enhancement measurements conducted on PCBM:MDMO-PPV blend films.

## V. CONCLUSIONS

We have measured the terahertz-frequency photoconductivity of two model polymer-fullerene blends, varying the incident fluence over four orders of magnitude. We observe a qualitatively similar time dynamic and terahertz-frequency conductivity spectrum upon photoexcitation at energies resonant with the peak of the  $\pi-\pi^*$  absorption and well below it. The values of  $\phi\mu$ , the quantum efficiency for charge generation multiplied by the carrier mobility, are comparable at these two photoexcitation energies, suggesting that the direct excitation of an intermediate charge-transfer complex is an efficient route to free charge generation. The time-averaged terahertz photoconductivity, obtained using a terahertz spectrometer based on a laser oscillator, reveal that the photoconductivity is enhanced by a factor of over 20 upon blending P3HT with PCBM. Finally, the fluence dependence of the photoconductivity demonstrate that different mechanisms for charge relaxation occur over different time scales; at early times ( $<1 \text{ ns}$ ) the linear dependence of photoconductivity upon fluence indicates that interfacial charge transfer dominates as an exciton decay pathway, generating charges with mobility of at least  $\sim 0.1 \text{ cm}^2 \text{ V}^{-1} \text{ s}^{-1}$ . At later times, a sub-linear relationship shows that carrier-carrier recombination effects influence the conductivity on a longer timescale ( $>1 \mu\text{s}$ ). Analysis of the time-averaged photoconductivity data suggests that the bimolecular charge annihilation constant for these blends is approximately two to three orders of magnitude smaller than that typical for neat polymer films, in accordance with a more stable charge-separated state for the blend system.

## ACKNOWLEDGMENTS

The authors acknowledge the assistance of Colin Johnston of the Materials Department (Oxford) with thin-film thickness measurements and the financial support of the Royal Society and the EPSRC-GB.

\*p.parkinson1@physics.ox.ac.uk

<sup>†</sup>l.herz@physics.ox.ac.uk

<sup>1</sup>M. B. Ketchen, D. Grischkowsky, T. C. Chen, C. C. Chi, I. N. Duling, N. J. Halas, J. M. Halbout, J. A. Kash, and G. P. Li, *Appl. Phys. Lett.* **48**, 751 (1986).

<sup>2</sup>R. H. Friend, R. W. Gymer, A. B. Holmes, J. H. Burroughes, R. N. Marks, C. Taliani, D. D. C. Bradley, J. L. Bredas, M. Logdlund, and W. R. Salaneck, *Nature (London)* **397**, 121 (1999).

<sup>3</sup>P. Peumans, A. Yakimov, and S. R. Forrest, *J. Appl. Phys.* **93**, 3693 (2003).

<sup>4</sup>Gang Li, Vishal Shrotriya, Jinsong Huang, Yan Yao, Tom Moriarty, Keith Emery, and Yang Yang, *Nat. Mater.* **4**, 864 (2005).

<sup>5</sup>K. Kim, J. Liu, M. A. G. Namboothiry, and D. L. Carroll, *Appl. Phys. Lett.* **90**, 163511 (2007).

<sup>6</sup>N. S. Sariciftci, L. Smilowitz, A. J. Heeger, and F. Wudl, *Science* **258**, 1474 (1992).

- <sup>7</sup>C. J. Brabec, F. Padinger, N. S. Sariciftci, and J. C. Hummelen, *J. Appl. Phys.* **85**, 6866 (1999).
- <sup>8</sup>Y. Kim, S. A. Choulis, J. Nelson, D. D. C. Bradley, S. Cook, and J. R. Durrant, *Appl. Phys. Lett.* **86**, 063502 (2005).
- <sup>9</sup>Y. Kim, S. Cook, S. M. Tuladhar, S. A. Choulis, J. N. J. R. Durrant, D. D. C. Bradley, M. Giles, I. McCulloch, C.-S. Ha, and M. Ree, *Nat. Mater.* **5**, 197 (2006).
- <sup>10</sup>L. M. Herz, C. Silva, R. T. Phillips, S. Setayesh, and K. Müllen, *Chem. Phys. Lett.* **347**, 318 (2001).
- <sup>11</sup>X. Ai, M. C. Beard, K. P. Knutsen, S. E. Shaheen, G. Rumbles, and R. J. Ellingson, *J. Phys. Chem. B* **110**, 25462 (2006).
- <sup>12</sup>H. Sirringhaus, P. J. Brown, R. H. Friend, M. M. Nielsen, K. Bechgaard, B. M. W. Langeveld-Voss, A. J. H. Spiering, R. A. J. Janssen, E. W. Meijer, and P. Herwig, *Nature (London)* **401**, 685 (1999).
- <sup>13</sup>Y. Zaushitsyn, V. Gulbinas, D. Zigmantas, F. Zhang, O. Inganäs, V. Sundström, and A. Yartsev, *Phys. Rev. B* **70**, 075202 (2004).
- <sup>14</sup>V. Gulbinas, Y. Zaushitsyn, H. Bässler, A. Yartsev, and V. Sundstrom, *Phys. Rev. B* **70**, 035215 (2004).
- <sup>15</sup>P. J. Brown, D. S. Thomas, A. Köhler, J. S. Wilson, J. S. Kim, C. M. Ramsdale, H. Sirringhaus, and R. H. Friend, *Phys. Rev. B* **67**, 064203 (2003).
- <sup>16</sup>T. J. Savenije, J. E. Kroeze, X. N. Yang, and J. Loos, *Thin Solid Films* **511-512**, 2 (2006).
- <sup>17</sup>P. Prins, F. C. Grozema, J. M. Schins, S. Patil, U. Scherf, and L. D. A. Siebbeles, *Phys. Rev. Lett.* **96**, 146601 (2006).
- <sup>18</sup>P. Prins, F. C. Grozema, J. M. Schins, T. J. Savenije, S. Patil, U. Scherf, and L. D. A. Siebbeles, *Phys. Rev. B* **73**, 045204 (2006).
- <sup>19</sup>G. Dicker, J. M. Warman, and L. D. A. Siebbeles, *J. Phys. Chem. B* **108**, 17818 (2004).
- <sup>20</sup>P. Prins, F. C. Grozema, and L. D. A. Siebbeles, *J. Phys. Chem. B* **110**, 14659 (2006).
- <sup>21</sup>E. Hendry, M. Koeberg, J. M. Schins, L. D. A. Siebbeles, and M. Bonn, *Chem. Phys. Lett.* **432**, 441 (2006).
- <sup>22</sup>E. Hendry, M. Koeberg, J. M. Schins, H. K. Nienhuys, V. Sundström, L. D. A. Siebbeles, and M. Bonn, *Phys. Rev. B* **71**, 125201 (2005).
- <sup>23</sup>E. Hendry, J. M. Schins, L. P. Candeias, L. D. A. Siebbeles, and M. Bonn, *Phys. Rev. Lett.* **92**, 196601 (2004).
- <sup>24</sup>M. Koeberg, E. Hendry, J. M. Schins, H. A. vanLaarhoven, C. F. J. Flipse, K. Reimann, M. Woerner, T. Elsaesser, and M. Bonn, *Phys. Rev. B* **75**, 195216 (2007).
- <sup>25</sup>P. D. Cunningham and L. M. Hayden, *J. Phys. Chem. C* **112**, 7928 (2008).
- <sup>26</sup>C. Soci, D. Moses, Q. H. Xu, and A. J. Heeger, *Phys. Rev. B* **72**, 245204 (2005).
- <sup>27</sup>A. C. Morteani, P. Sreearunothai, L. M. Herz, R. H. Friend, and C. Silva, *Phys. Rev. Lett.* **92**, 247402 (2004).
- <sup>28</sup>P. Sreearunothai, A. C. Morteani, I. Avilov, J. Cornil, D. Beljonne, R. H. Friend, R. T. Phillips, C. Silva, and L. M. Herz, *Phys. Rev. Lett.* **96**, 117403 (2006).
- <sup>29</sup>O. Esenturk, J. S. Melinger, and E. J. Heilweil, *J. Appl. Phys.* **103**, 023102 (2008).
- <sup>30</sup>H. Nemeč, H. K. Nienhuys, F. Zhang, O. Inganäs, A. Yartsev, and V. Sundström, *J. Phys. Chem. C* **112**, 6558 (2008).
- <sup>31</sup>C. Tanase, E. J. Meijer, P. W. M. Blom, and D. M. deLeeuw, *Phys. Rev. Lett.* **91**, 216601 (2003).
- <sup>32</sup>L. Duvillaret, F. Garet, and J. L. Coutaz, *Appl. Opt.* **38**, 409 (1999).
- <sup>33</sup>E. Hendry, Ph.D. thesis, Universiteit van Amsterdam, 2005.
- <sup>34</sup>L. Goris, A. Poruba, L. Hod'akova, M. Vanecek, K. Haenen, M. Nesladek, P. Wagner, D. Vanderzande, and J. V. Manca, *Appl. Phys. Lett.* **88**, 052113 (2006).
- <sup>35</sup>J. J. Benson-Smith, L. Goris, K. Vandewal, K. Haenen, J. V. Manca, D. Vanderzande, D. D. C. Bradley, and J. Nelson, *Adv. Funct. Mater.* **17**, 451 (2007).
- <sup>36</sup>J. Lloyd-Hughes, S. K. E. Merchant, L. Fu, H. H. Tan, C. Jagadish, E. Castro-Camus, and M. B. Johnston, *Appl. Phys. Lett.* **89**, 232102 (2006).
- <sup>37</sup>K. P. H. Lui and F. A. Hegmann, *Appl. Phys. Lett.* **78**, 3478 (2001).
- <sup>38</sup>T. I. Jeon, D. Grischkowsky, A. K. Mukherjee, and R. Menon, *Appl. Phys. Lett.* **79**, 4142 (2001).
- <sup>39</sup>T. I. Jeon, D. Grischkowsky, A. K. Mukherjee, and R. Menon, *Appl. Phys. Lett.* **81**, 2902 (2002).
- <sup>40</sup>H. Scher and E. W. Montroll, *Phys. Rev. B* **12**, 2455 (1975).
- <sup>41</sup>M. C. Beard, G. M. Turner, and C. A. Schmuttenmaer, *Phys. Rev. B* **62**, 15764 (2000).
- <sup>42</sup>T. I. Jeon, D. Grischkowsky, A. K. Mukherjee, and R. Menon, *Appl. Phys. Lett.* **77**, 2452 (2000).
- <sup>43</sup>T. I. Jeon, D. Grischkowsky, A. K. Mukherjee, and R. Menon, *Synth. Met.* **135-136**, 451 (2003).
- <sup>44</sup>F. C. Grozema, Y. A. Berlin, M. A. Ratner, and L. D. A. Siebbeles, *J. Phys. Chem. B* **106**, 7791 (2002).
- <sup>45</sup>N. V. Smith, *Phys. Rev. B* **64**, 155106 (2001).
- <sup>46</sup>P. Parkinson, J. Lloyd-Hughes, Q. Gao, H. H. Tan, C. Jagadish, M. B. Johnston, and L. M. Herz, *Nano Lett.* **7**, 2162 (2007).
- <sup>47</sup>C. X. Sheng, M. Tong, S. Singh, and Z. V. Vardeny, *Phys. Rev. B* **75**, 085206 (2007).
- <sup>48</sup>I. W. Hwang, C. Soci, D. Moses, Z. G. Zhu, D. Waller, R. Gaudiana, C. J. Brabec, and A. J. Heeger, *Adv. Mater. (Weinheim, Ger.)* **19**, 2307 (2007).
- <sup>49</sup>M. A. Loi, S. Toffanin, M. Muccini, M. Forster, U. Scherf, and M. Scharber, *Adv. Funct. Mater.* **17**, 2111 (2007).
- <sup>50</sup>M. Pope and C. E. Swenberg, in *Electronic Processes in Organic Crystals and Polymers*, Monographys on the Physics and Chemistry of Materials, 2nd ed. (Oxford Science, New York, 1999).
- <sup>51</sup>S. Barth, H. Bässler, H. Rost, and H. H. Hörhold, *Phys. Rev. B* **56**, 3844 (1997).
- <sup>52</sup>S. Barth and H. Bässler, *Phys. Rev. Lett.* **79**, 4445 (1997).
- <sup>53</sup>S. Barth, H. Bässler, U. Scherf, and K. Müllen, *Chem. Phys. Lett.* **288**, 147 (1998).
- <sup>54</sup>M. Wohlgenannt, W. Graupner, G. Leising, and Z. V. Vardeny, *Phys. Rev. Lett.* **82**, 3344 (1999).
- <sup>55</sup>V. I. Arkhipov, E. V. Emelianova, and H. Bässler, *Phys. Rev. Lett.* **82**, 1321 (1999).
- <sup>56</sup>C. Silva, A. S. Dhoot, D. M. Russell, M. A. Stevens, A. C. Arias, J. D. MacKenzie, N. C. Greenham, R. H. Friend, S. Setayesh, and K. Müllen, *Phys. Rev. B* **64**, 125211 (2001).
- <sup>57</sup>A. Köhler, D. Beljonne, Z. Shuai, J. L. Bredas, A. B. Holmes, A. Kraus, K. Müllen, and R. H. Friend, *Nature (London)* **392**, 903 (1998).
- <sup>58</sup>L. Onsager, *Phys. Rev.* **54**, 554 (1938).
- <sup>59</sup>G. Dicker, M. P. de Haas, L. D. A. Siebbeles, and J. M. Warman, *Phys. Rev. B* **70**, 045203 (2004).
- <sup>60</sup>J. Lloyd-Hughes, T. Richards, H. Sirringhaus, M. B. Johnston, and L. M. Herz, *Phys. Rev. B* **77**, 125203 (2008).
- <sup>61</sup>A. Ruseckas, M. Theander, M. R. Andersson, M. Svensson, M. Prato, O. Inganäs, and V. Sundström, *Chem. Phys. Lett.* **322**, 136 (2000).

- <sup>62</sup>I. W. Hwang, D. Moses, and A. J. Heeger, *J. Phys. Chem. C* **112**, 4350 (2008).
- <sup>63</sup>S. V. Frolov, Z. Bao, M. Wohlgenannt, and Z. V. Vardeny, *Phys. Rev. Lett.* **85**, 2196 (2000).
- <sup>64</sup>W. Graupner, G. Cerullo, G. Lanzani, M. Nisoli, E. J. W. List, G. Leising, and S. DeSilvestri, *Phys. Rev. Lett.* **81**, 3259 (1998).
- <sup>65</sup>C. Gadermaier, G. Cerullo, G. Sansone, G. Leising, U. Scherf, and G. Lanzani, *Phys. Rev. Lett.* **89**, 117402 (2002).
- <sup>66</sup>J. G. Müller, U. Lemmer, J. Feldmann, and U. Scherf, *Phys. Rev. Lett.* **88**, 147401 (2002).
- <sup>67</sup>J. G. Müller, J. M. Lupton, J. Feldmann, U. Lemmer, M. C. Scharber, N. S. Sariciftci, C. J. Brabec, and U. Scherf, *Phys. Rev. B* **72**, 195208 (2005).
- <sup>68</sup>X. P. Zhang, Y. J. Xia, R. H. Friend, and C. Silva, *Phys. Rev. B* **73**, 245201 (2006).
- <sup>69</sup>S. E. Shaheen, C. J. Brabec, N. S. Sariciftci, F. Padinger, T. Fromherz, and J. C. Hummelen, *Appl. Phys. Lett.* **78**, 841 (2001).
- <sup>70</sup>A. Pivrikas, G. Juška, A. J. Mozer, M. Scharber, K. Arlauskas, N. S. Sariciftci, H. Stubb, and R. Österbacka, *Phys. Rev. Lett.* **94**, 176806 (2005).
- <sup>71</sup>G. Juška, G. Sliaužys, K. Genevičius, K. Arlauskas, A. Pivrikas, M. Scharber, G. Dennler, N. S. Sariciftci, and R. Österbacka, *Phys. Rev. B* **74**, 115314 (2006).
- <sup>72</sup>J. Piris, N. Kopidakis, D. C. Olson, S. E. Shaheen, D. S. Ginley, and G. Rumbles, *Adv. Funct. Mater.* **17**, 3849 (2007).
- <sup>73</sup>M. Caironi, T. Agostinelli, D. Natali, M. Sampietro, R. Cugola, M. Catellani, and S. Luzzati, *J. Appl. Phys.* **102**, 024503 (2007).
- <sup>74</sup>M. Theander, A. Yartsev, D. Zigmantas, V. Sundstrom, W. Mammo, M. R. Andersson, and O. Inganäs, *Phys. Rev. B* **61**, 12957 (2000).
- <sup>75</sup>Y. Kim, H. J. Joyce, O. Gao, H. H. Tan, C. Jagadish, M. Paladugu, J. Zou, and A. A. Suvorova, *Nano Lett.* **6**, 599 (2006).